Nanoscale

Check for updates

Self-assembly pathways and polymorphism in peptide-based nanostructures†

Nikola A. Dudukovic, [iD] *[a,b] Benjamin C. Hudson,[c] Anant K. Paravastu[c] and Charles F. Zukoski[d]

Dipeptide derivative molecules can self-assemble into space-filling nanofiber networks at low volume fractions (<1%), allowing the formation of molecular gels with tunable mechanical properties. The self-assembly of dipeptide-based molecules is reminiscent of pathological amyloid fibril formation by naturally occurring polypeptides. Fluorenylmethoxycarbonyl-diphenylalanine (Fmoc-FF) is the most widely studied such molecule, but the thermodynamic and kinetic phenomena giving rise to Fmoc-FF gel formation remain poorly understood. We have previously presented evidence that the gelation process is a first order phase transition characterized by low energy barriers to nucleation, short induction times, and rapid quasi-one-dimensional crystal growth, stemming from solvent–solute interactions and highly specific molecular packing. Here, we discuss the phase behavior of Fmoc-FF in different solvents. We find that Fmoc-FF gel formation can be induced in apolar solvents, in addition to previously established pathways in aqueous systems. We further show that in certain solvent systems anisotropic crystals (nanofibers) are an initial metastable state, after which macroscopic crystal aggregates with no preferred axis of growth are formed. The molecular conformation is sensitive to solvent composition during assembly, indicating that Fmoc-FF may be a simple model system to study complex thermodynamic and kinetic phenomena involved in peptide self-assembly.

Introduction

The phase behavior of mixtures containing self-organizing molecules is a sustained challenge in molecular purifications and in the study of molecular structure. A number of studies have shown that generalized phase diagrams can be used to understand the general features of a binary mixture of solute and solvent.[1–3] In some systems, however, it is not clear whether phase separation is determined primarily by thermodynamics or kinetics.[4–7] In the thermodynamic limit, if solute molecules are assumed to experience a net attraction of ε, a phase diagram could be developed where kT/ε (experimentally characterized by measuring solute secondary virial coefficients and solute self-diffusivity)[8–12] is plotted as a function of solute volume
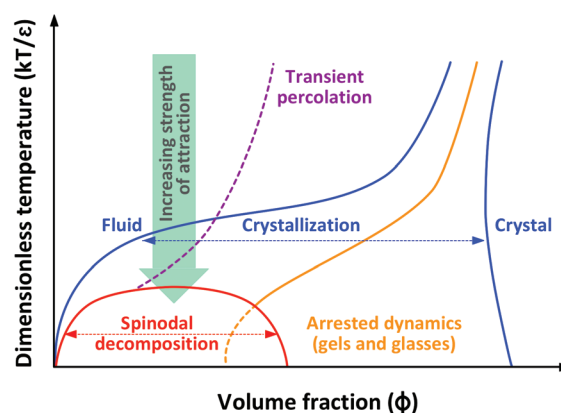

Fig. 1 Illustration of a typical colloidal phase diagram.

fraction (Fig. 1). These generalized phase diagrams have been shown to be useful predictors of solubility of small molecules, proteins and colloids, and, surprisingly, capture solubilities even when the molecules have very anisotropic interactions.[10–12] The general nature of the proposed phase diagram suggests that at the same value of ε/kT, different solutes will have the same solubility. Solvent–solute interactions play a key role in establishing the magnitude of ε/kT. These attractions are often broken down into polar, dispersion and hydrogen bonding interactions. The relative

[a]Lawrence Livermore National Laboratory, P.O. Box 808, Livermore, CA 94551, USA. E-mail: dudukovic1@llnl.gov
[b]Department of Chemical and Biomolecular Engineering, University of Illinois at Urbana-Champaign, Urbana, IL 61801, USA
[c]School of Chemical & Biomolecular Engineering, Georgia Institute of Technology, Atlanta, GA 30332, USA
[d]Chemical and Biological Engineering, University at Buffalo, Buffalo, NY 14260, USA
†Electronic supplementary information (ESI) available. See DOI: 10.1039/c7nr06724k

nature of these interactions can control molecular packing within the solute structure.

Self-assembling gelators based on short peptide derivative molecules form ordered fibrous structures, commonly *via* π–π stacking and hydrogen bonding interactions.[13–22] The resulting bulk properties of the produced materials are characteristic of soft solids. The most widely studied such gelator molecule is fluorenylmethoxycarbonyl-diphenylalanine (Fmoc-FF).[13–21] Low-concentration solutions of Fmoc-FF form gels of substantial elastic moduli when mixed with water. Because of their flexibility for altering chemical composition, Fmoc-FF and similar short peptide derivative gelators show promise for a host of uses including tissue engineering, nanofabrication, energy storage, photoelectronics, and biosensing.[23–27] However, the design of new gelator molecules with desired self-assembly properties is limited by the lack of understanding of the gelation mechanism. Hence, these low molecular weight gelators are less often designed than they are discovered.

We have previously shown that gelation of Fmoc-FF in DMSO solutions triggered by addition of water results from a first order phase transition giving rise to elongated crystals of high aspect ratios.[21] Detailed studies indicate that increasing the concentration of water increases the strength of attraction ε/kT, leading to fast nucleation rates and quasi-one-dimensional crystal growth.[21] If this is done with sufficient rapidity, the mixture will lie below the spinodal and large amorphous droplets will form, which over time re-dissolve, nucleate and grow crystals in coexistence with a dilute solution.

However, the type of solvent can impact the molecular packing of crystals formed when the solidus is crossed. As we show here, solvent–solute interactions determine the self-assembly pathway and structure stability, and therefore play a crucial role in shaping the energy landscape and phase behavior of dipeptide gelators. Understanding these interactions is necessary not only for developing guidelines for adequate solvent environments for existing gelators, but moreover for generalizing the design rules for novel self-assembling molecules. In addition, widely studied peptides such as Aβ-42, the Alzheimer's peptide and initial inspiration for study of Fmoc-FF, yield highly polymorphic assemblies. Polymorphism in these systems is assumed to be the result of kinetic trapping, rather than relaxation to thermodynamic equilibrium. Hence, Fmoc-FF may present us with an opportunity to not only shed light upon a highly versatile biomaterial, but to also a near-equilibrium, self-assembled structure of an amino acid motif thought to be crucial to the self-assembly of Aβ-42.

With the exception of a few notable studies, the role of solvents in dipeptide gelation has been largely overlooked in the literature. Raeburn *et al.* investigated gels of Fmoc-FF in four different solvents mixed with water, reporting their observations on the resulting mechanical properties.[28] Wang *et al.* investigated the role of solvent-bridged hydrogen bonding in fiber formation of diphenylalanine (FF).[29] Ramos Sasselli *et al.* have developed a simple packing model based on solvophobicity of amphiphilic molecules to determine the thermo-

dynamic favorability of fiber stability and applied it to pH-triggered gelation of Fmoc-FF. Previous studies highlighting fiber *versus* crystal formation have focused on the structure of different gelator molecules in a fixed system[31,32] (pH-triggered gelation in aqueous solution); here, we instead explore the phase behavior of one molecule in a variety of solvent systems with the aim of understanding what drives the formation of fibrous gels. While many studies have focused only on biocompatible hydrogels, we employ a multitude of solvents with a range of different interaction types, mainly in order to recognize how these interactions lead to specific phase behavior and stability, as well as to develop guidelines for applications that do not require cell-friendly solvents.

Predicting the effects of solvents on both solubility and morphology of precipitates remains a challenge. One method to address these issues is to use Hansen solubility parameters (HSPs from hereon) that characterize solvent properties by accounting for three types of molecular interactions: polar (δ_p), capacity to form hydrogen bonds (δ_h), and strength of dispersive or van der Waals interactions (δ_d).[33] Any given solvent for which these three parameters are known can be represented as a point in a 3D space in which the axes are defined by δ_h, δ_p and δ_d, referred to as the Hansen space. The solubility of a solute A in solvent B is expected to be inversely proportional to the distance R between the two points in the Hansen space:[33]

$$R = \sqrt{(\delta_p^A - \delta_p^B)^2 + (\delta_h^A - \delta_h^B)^2 + 4(\delta_d^A - \delta_d^B)^2}. \tag{1}$$

The larger the value of R, the less soluble A will be in B. Estimated solubility parameters can be calculated based on group contributions of the molecule.[33,34] Experimentally, they are established by finding a number of solvents in which the substance is soluble or insoluble, plotting their coordinates in Hansen space, and determining a sphere that encompasses as many solvents as possible in which the solute dissolves. The coordinates of the center of that solubility sphere are then considered to be the HSPs of the solute.[33,35] Outside of the solubility sphere, other domains containing information about phase behavior can be established.[36–41] We employ this approach to study the phase behavior of Fmoc-FF and interpret the solvent–solute interactions present in the system. Three solvent systems (DMSO/H$_2$O, methanol/H$_2$O, and toluene) are selected to illustrate distinct phase behavior and highlight structural differences. Our findings indicate that:

(1) Gels can be produced by thermal effects in the absence of water in highly apolar solvents.

(2) Fmoc-FF exhibits distinct polymorphism in certain solvent systems, where it can transition from a metastable anisotropic crystalline structure (fibers) to large crystal aggregates with no preferred axis of growth.

(3) The molecular packing of Fmoc-FF in fibers differs across solvents.

(4) Multiple populations of fibers with different molecular order can exist in a single system.

(5) The observed phase behavior can be understood in terms of HSPs as a measure of solvent–solute interactions.

Experimental

Sample preparation

All non-NMR samples were prepared at a fixed Fmoc-FF concentration of 15 mg mL^{-1} (minimum concentration to ensure a sufficient signal in the CPMAS NMR measurements). The appropriate mass of the solid peptide was added to 1 mL of solvent and vortex-mixed. In some cases, the suspension was heated (to no more than 75 °C) to facilitate dissolution. If Fmoc-FF did not form a clear solution at this temperature, the behavior in the given solvent was labeled as "insoluble". The heated solutions were allowed to cool back to room temperature and left to stand overnight, after which the phase behavior was noted. For ternary systems, the desired mass of Fmoc-FF was first fully dissolved in the solvent, followed by addition of the appropriate amount water, and left to stand overnight. NMR samples were allowed to self-assemble in the following solvent systems: DMSO/H$_2$O (x_{H_2O} = 0.95), methanol/H$_2$O (x_{H_2O} = 0.95 and x_{H_2O} = 0.20), pure methanol (no H$_2$O), and pure toluene. Each sample was prepared at a concentration of 15 mg mL^{-1}, with the exception of the sample in pure methanol, which was prepared at approximately 300 mg mL^{-1}.

Confocal fluorescence microscopy

A small amount (40 ppm) of Nile Blue fluorescent dye was added to the solution. Immediately upon mixing the solution with water, 50 μL of the mixture was transferred into a glass bottom dish (MatTek Corp.) and covered with a lid. The sample was loaded onto a Zeiss LSM 700 confocal microscope and images were taken using a 63× magnification oil immersion objective at 639 nm excitation wavelength. In the case of solvents in which the dye was insoluble (apolar solvents such as benzene and toluene), the peptide was pre-dyed. This procedure involved dissolving the Fmoc-FF and dye in a highly volatile solvent (acetone) and heating the solution under vacuum until all the solvent had evaporated. The dyed solid powder was then dissolved in the desired apolar solvent.

Transmission electron microscopy

A 15 μL droplet of the solution was transferred onto a glass surface, before the onset of gel transition. A 400 mesh carbon coated copper grid (SPI Supplies) was placed on the sample droplet for 30 s and the excess liquid was removed. The grid was then washed and placed on a 15 μL droplet of ammonium molybdate solution for 60 s. The excess stain was washed and the sample grid was stored covered overnight. Images were collected using JEOL 2100 Cryo and JEOL 2010 LaB6 transmission electron microscopes operating at 200 kV.

Solid state NMR spectroscopy

All NMR experiments were performed on a 500 MHz (11.75 T) Bruker NMR spectrometer. All samples were prepared as described previously and lyophilized. We used ^{1}H–^{13}C cross polarization magic angle spinning (CPMAS) solid-state NMR to probe the natural abundance ^{13}C populations of Fmoc-FF assemblies.[42] The shapes and linewidths of CPMAS NMR signals can be used to assess the overall level of molecular order. The peaks from the Fmoc group were identified by running CPMAS on two samples assembled in DMSO/H$_2$O (x_{H_2O} = 0.95), one of which was uniformly labeled with ^{13}C isotopes on the two phenylalanine residues (see Fig. S1, ESI†). Each sample was packed into a 3.2 mm Bruker NMR rotor. The magic angle spinning speed for each experiment was 20 kHz. A 2 ms ^{1}H–^{13}C CP spinlock was applied concurrently with a 50 kHz radio frequency field on the ^{13}C channel and linear ramp pulse between 60 and 120 kHz on the ^{1}H channel. During signal acquisition, a 100 kHz ^{1}H decoupling pulse was applied using two pulse phase modulation (TPPM).[43] Each spectrum was collected over the course of 12–15 hours of signal averaging time with a recycle delay of 5 s. The NMR chemical shifts were referenced to adamantane. All measurements were repeated to ensure reproducibility.

Results and discussion

Phase behavior observations

The solubility of Fmoc-FF at a concentration of 15 mg mL^{-1} was tested in 15 different solvents and mixtures of solvents with water. The outcomes, which were reproducible across all solvents, are classified in the following categories:

- **Liquid:** Fmoc-FF fully dissolves in the solvent and remains a stable, colorless solution after equilibrating at room temperature overnight (Fig. 2a).
- **Gel:** Fmoc-FF fully dissolves in the solvent when heated up to 75 °C and forms a gel upon cooling to room temperature, or upon addition of water (Fig. 2b).
- **Crystal:** Fmoc-FF fully dissolves, but overnight macroscopic crystals are grown either from the solution (Fig. 2c) or from the gel phase (Fig. 2d).
- **Insoluble:** The Fmoc-FF powder does not dissolve in the solvent at the given concentration even when the suspension is heated to 75 °C (Fig. 2e).

The investigated solvents, corresponding HSPs, and resulting phase behavior in the binary Fmoc-FF/solvent system are summarized in Table 1. The solvents can be represented as points in the Hansen space with coordinates ($δ_h$, $δ_p$, $2δ_d$) (Fig. 3a). The points are assigned different colors to indicate the phase behavior of Fmoc-FF (blue: liquid, red: gel, green: crystals, black: insoluble). The results for ternary systems (Fmoc-FF/solvent/H$_2$O) are summarized in Table 2 and presented graphically in Hansen space in Fig. 3b. The HSPs for
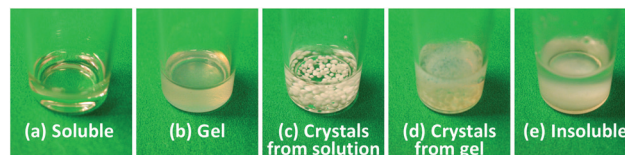

Fig. 2 Examples of observed Fmoc-FF phase behavior in various solvents.

(a) Soluble   (b) Gel   (c) Crystals from solution   (d) Crystals from gel   (e) Insoluble

Table 1 Hansen solubility parameters of the investigated solvents and resulting phase behavior of binary systems with Fmoc-FF

| No.	Solvent	δ_h	δ_p	δ_d	Result
1	Dimethyl sulfoxide (DMSO)	4.99	8.02	9.00	Liquid
2	Acetone	3.42	6.08	7.58	Liquid
3	Dimethyl formamide (DMF)	6.52	6.70	8.51	Liquid
4	Hexafluoroisopropanol (HFIP)	13.89	2.41	14.17	Liquid
5	Tetrahydrofuran (THF)	3.91	2.79	8.21	Liquid
6	Methanol	10.9	6.01	7.38	Crystal
7	Ethanol	9.48	4.30	7.72	Crystal
8	Acetonitrile	2.98	8.80	7.48	Crystal
9	Benzene	0.98	0.00	9.00	Gel
10	Toluene	0.98	0.68	8.80	Gel
11	Chloroform	0.00	0.00	17.8	Gel
12	Dichloromethane	2.98	3.08	8.90	Gel
13	Hexane	0.00	0.00	7.28	Insoluble
14	Cyclohexane	6.60	2.00	8.51	Insoluble
15	Water	20.68	7.82	7.63	Insoluble

solvent/water mixtures are calculated by assuming a linear relationship:[36]

$$\delta_{mixture} = x_{H_2O}\delta_{H_2O} + (1 - x_{H_2O})\delta_{solvent} \qquad (2)$$

where x_{H_2O} is the concentration (v/v) of water in the mixture.

The first major observation from these investigations is that gels can be produced in the absence of water. This is evi-

denced in apolar and borderline-polar solvents (benzene, toluene, chloroform, and dichloromethane), in which Fmoc-FF self-assembles into a fibrous network similar to those seen in ternary systems (Fig. 4). The gel transition is very rapid in benzene and toluene (<1 min) and somewhat slower (~30 min) in chloroform and dichloromethane. No signs of amorphous precipitate formation are observed in any of these solvents, which suggests that the temperature quench is sufficiently slow to avoid the possibility of crossing of the phase separation boundary at this volume fraction, but rapid enough to achieve nucleation at short induction times in benzene and toluene.[21] The second interesting outcome is the formation of large crystal aggregates with no preferred axis of growth, observed in certain mixtures of water with methanol, ethanol, DMF, and HFIP. At low water concentrations, signs of an amorphous white precipitate are shown, after which the solution quickly becomes clear again and floating crystals are nucleated from the solution (Fig. 2c) at induction times on the order of hours (days in DMF). This indicates redissolution of the amorphous precipitate places the system at a point where the solubility boundary is crossed and crystallization takes over (Fig. 1). The fact that macroscopic crystals are grown instead of nanofibers of high aspect ratios suggests that the surface energies of the ends and sides of the crystal are similar, the barrier to nucleation is high and long induction times are observed, which is
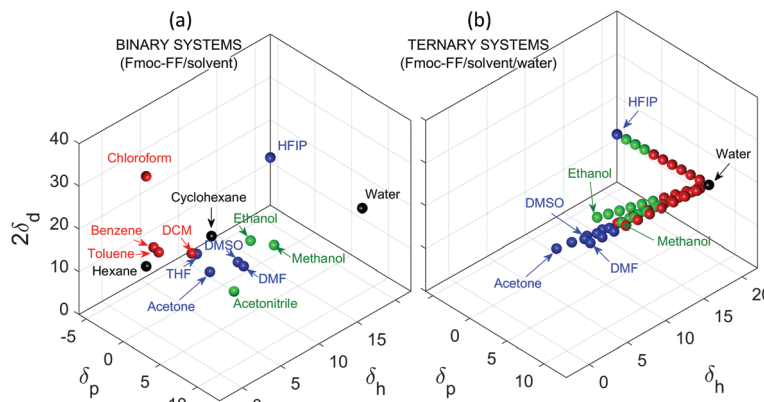
Fig. 3 Phase behavior of Fmoc-FF in (a) pure solvents and (b) mixtures of select solvents and water represented in Hansen space (black: insoluble, blue: soluble, red: gel, green: crystals).

Table 2 Phase behavior of Fmoc-FF in ternary aqueous systems. The corresponding HSPs are calculated as given in eqn (2)

| x_{H_2O}	DMSO	Acetone	DMF	Methanol	Ethanol	HFIP
0	Liquid	Liquid	Liquid	Crystal	Crystal	Liquid
0.1	Liquid	Liquid	Liquid	Crystal	Crystal	Crystal
0.2	Liquid	Liquid	Liquid	Crystal	Crystal	Crystal
0.3	Gel	Liquid	Liquid	Crystal	Crystal	Crystal
0.4	Gel	Gel	Crystal	Crystal	Crystal	Gel
0.5	Gel	Gel	Crystal	Crystal	Crystal	Gel
0.6	Gel	Gel	Crystal	Gel	Gel	Gel
0.7	Gel	Gel	Gel	Gel	Gel	Gel
0.8	Gel	Gel	Gel	Gel	Gel	Gel
0.9	Gel	Gel	Gel	Gel	Gel	Gel
1	Insoluble	Insoluble	Insoluble	Insoluble	Insoluble	Insoluble
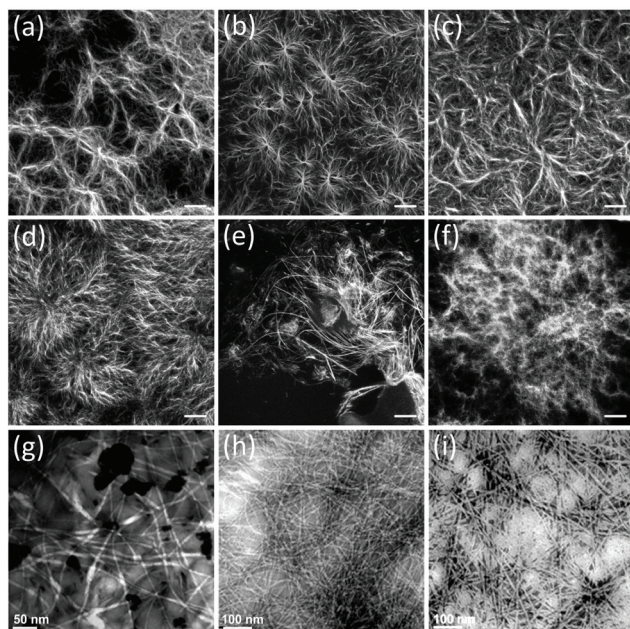
Fig. 4 (a–f) Confocal microscopy images of Fmoc-FF gels in: (a) DMSO/H$_2$O, (b) acetone/H$_2$O, (c) methanol/H$_2$O, (d) HFIP/H$_2$O, (e) benzene, (f) toluene. Scale bars represent 10 μm. (g–i) TEM images of Fmoc-FF gels in (g) DMSO/H$_2$O, (h) methanol/H$_2$O, and (i) toluene.
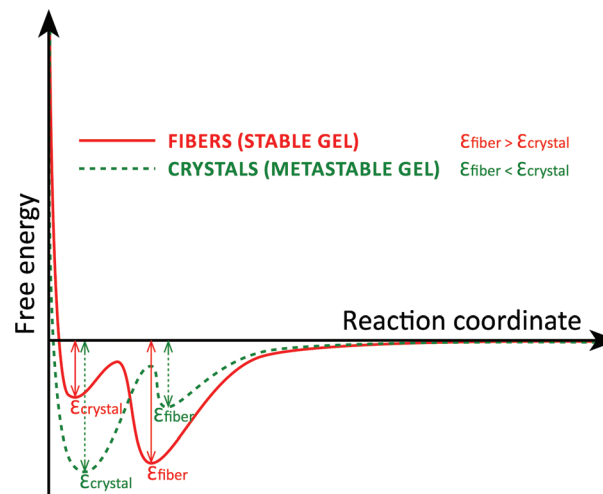

Fig. 5 Illustration of the energy landscape of Fmoc-FF in different systems. Red: the lowest free energy minimum corresponds to fibers, and the gel is stable. Green: fibers are metastable, and large crystal growth proceeds when the barrier between the minima is overcome.

consistent with the ideas presented in our previous publication.[21]

Upon addition of moderate water concentrations, a clear gel is formed as the amorphous precipitate dissolves within less than 5 minutes. Over a time of several hours, large crystals are grown from the gel phase (Fig. 2d). In methanol and ethanol, over long times (hours to days) the fibrous gel phase disappears completely and millimeter-sized crystals are left suspended in solution, indicating low crystal density and possible incorporation of solvent in the crystal structure.

Based on the presented observations, it is clear that Fmoc-FF has at least two distinct polymorphs – elongated nanofibers and large crystals with no preferred axis of growth. Ostwald's law of stages suggests that the polymorph that crystallizes first is the least stable.[44,45] In light of this, as well as the ideas introduced previously,[21,30,46–48] we conclude that the nucleation barrier to the formation of fibers is low, thus driving the initial formation of fibers at short induction times. The subsequent transition can occur either due to: (a) nucleation from the remaining free molecules in solution at longer induction times, or (b) from the breakdown and aggregation of existing fibers. Mechanism (a) would imply that once the high nucleation barrier for growth of large crystals is overcome, the subsequent crystalline structure would be at a lower free energy minimum (Fig. 5). The growth of these larger structures then presumably proceeds following an Ostwald ripening process in which the crystals are grown at the expense of the fibers as the molecules try to minimize their surface area.[44] Mechanism (b) would suggest that the side interactions between fibers are strong and that local restructuring can take place as the fibers

come together.[49] SEM images of large crystals grown from the Fmoc-FF/methanol/water gel phase (Fig. S2, ESI†) indicate that these are aggregates of smaller rod-like crystals of diameters much larger (∼1 μm) and aspect ratios much lower than those of nanofibers in the gel phase, which supports the possibility of lateral interactions of nanofibers in the restructuring process.

Structural differences in fibers

It is important to note that, aside from the evident difference between anisotropic and isotropic crystals, multiple distinct fiber structure populations exist across Fmoc-FF systems from different solvents and likely within samples from the same solvent. CPMAS NMR data (Fig. 6) shows substantial changes in chemical shift across the different solvent systems in areas known to be sensitive to structural change in peptide systems. Fig. 6b shows the carbonyl region of Fig. 6a, in which there are two significant peaks in each spectrum due to the carbonyl groups of the phenylalanine residues. From the DMSO sample, we see two peaks at about 172.5 and 174 ppm corresponding to chemical shift values of protonated carboxylic acids. However, in both methanol samples and the toluene sample, there is a clear shift in one peak from 174 to 179 ppm. We believe the peak near 179 ppm is the deprotonated C-terminus of the molecule. The same peak shifting behavior can be seen in the aromatic and aliphatic regions of the spectra. Fig. 6c shows two peaks between 139 and 135 ppm, corresponding to the γ-carbons of the two phenylalanine residues, the only aromatic carbon atoms capable of substantial conformational variation. Each spectrum has a peak at about 136 ppm, but intensity varies across each solvent. The second peak in each spectrum is of variable intensity and falls between 137 and 138 ppm. In this peak however, the position is shifted slightly to the right in the methanol samples compared to the DMSO
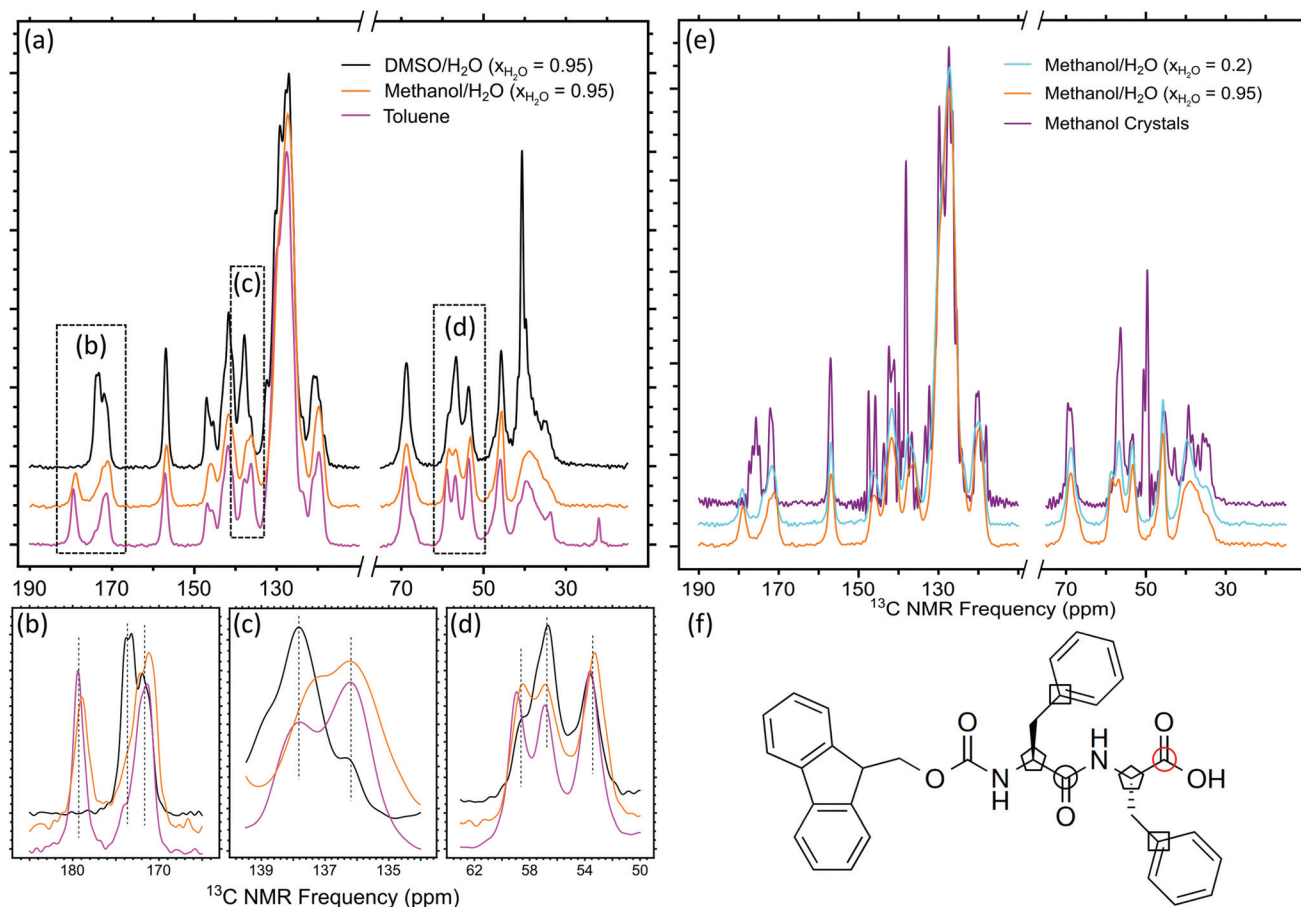
Fig. 6 (a) CPMAS spectra obtained from Fmoc-FF nanofibers self-assembled in DMSO/H₂O, methanol/H₂O, and toluene; (b–d) carbonyl, γ-carbon, and α-carbon signals of each spectrum; (e) comparison of spectra obtained from fibers and crystals in different methanol-based systems; (f) chemical structure of Fmoc-FF with carbonyls circled (panel b, the red circle indicates the C-terminus), g-carbons boxed (panel c), and a-carbons in pentagons (panel d).

and toluene samples. Fig. 6d shows the α-carbon signals of the phenylalanine residues. Moving downward from DMSO to toluene in Fig. 6d, we can see the clear growth of a third peak which appears in the DMSO spectrum as only a small "shoulder" on the large peak near 57 ppm. Also, unlike in Fig. 6b and c, we see three significant α-carbon signals. This suggests a significant contribution from three α-carbon conformational populations, where the fraction of each is dependent on the solvent environment of gelation. This suggests the presence of multiple distinct and well-ordered molecular conformations within these gels. Finally, there is a very sharp and intense peak in the DMSO spectrum at about 38 ppm. We believe this is a β-carbon signal from the phenylalanine residues. In other solvents, the magnitude of the peak is much lower and broader relative to DMSO. However, the intensity of this peak varies significantly across multiple gel samples formed in DMSO, indicating some degree of polymorphism at this site.

The spectrum obtained Fmoc-FF crystals formed in methanol (Fig. 6e) confirmed that the structures were crystalline (and not amorphous), as evidenced in the very sharp lines com-

pared to the gel samples, and the signal truncation we see when the CPMAS is run with the same recycle delay used in all of our other experiments. The CPMAS spectrum of Fmoc-FF crystals formed in pure methanol differs from the methanol fiber spectra at multiple points. First, there is a broad peak at ~177 ppm which is not present in any of fiber samples tested, likely from the C-terminus of the molecule. The peak splits at multiple points, indicating that the C-terminus at least may have freedom to adopt a set of different conformations. Furthermore, unlike the both methanol fiber samples and the toluene sample, there are only two major signals from α-carbon populations. Additionally, in the aliphatic region of the spectrum, we see a sharp signal at ~50 ppm. This is the expected approximate position for the methyl group of methanol, likely indicating that the methanol itself is integrated into the Fmoc-FF crystal structure. This presence of solvent in the structure was not observed in either of the methanol gel samples, though it is possible the freeze-drying method used on the gel samples removed methanol from the fiber structure. However, this is unlikely because the dried material still appears to be in an ordered conformation.

The data presented here are not sufficient to offer a definitive hypothesis of complete molecular structure and conformation, but there is obvious, systematic signal variation between solvent environments. Though Fmoc-FF is not by definition a peptide, variation of peptide carbonyl and α-carbon signals in particular are known to be strong indicators of change in peptide secondary structure. In addition to variation in the carbonyl and α-carbon regions of the spectra, the slight shift in peak position of the aromatic signal between 137 and 138 ppm is likely an indication that one of the γ-carbon populations adopts a different conformation in the methanol samples as compared to the DMSO and toluene samples. The γ-carbon shift, along with β-carbon signal variation across each sample, may be an indication of variation in hydrophobic packing of the phenylalanine sidechains.

It is also worth comparing the Fmoc-FF structural variability with solvent similarity. This can be most easily observed by comparing the spectra from DMSO (x_{H_2O} = 0.95), methanol (x_{H_2O} = 0.95), and toluene. The samples from DMSO and methanol self-assemble is what are principally equivalent solvents. Each begins from solution and is triggered by the addition of water to the system. The sample from toluene assembles in a highly apolar environment and without the need for a trigger. Yet Fig. 6b–d all show similar peak positions for the methanol (x_{H_2O} = 0.95) and toluene samples, with the DMSO signals deviating significantly from these two. Similar peak positions in the CPMAS spectra are not sufficient to conclude that we are seeing similarities in the fiber structures of the methanol and toluene samples. However, differences in peak position are sufficient to conclude that we are observing differences in fiber structure. We believe this may be an indication of kinetic trapping playing a role in the determination of the fiber conformation, as in classical amyloid systems.[4–7]

Interpretation of phase behavior – domains in Hansen space

In order to clarify the conditions under which the observed phase behavior occurs, we define spherical domains in the Hansen space that capture solubility, gelation, and crystal formation. Typically, spheres indicating different phase behavior are defined concentrically around the HSP coordinates of the solute and the solubility is described by the distance R in eqn (1).[33,35] However, more than one gelation sphere can be observed and that different structures can be formed in different domains in the Hansen space.[38] (The domains do not have to be spherical, but spheres are commonly used as the simplest approximation.)

Raghavan *et al.* have developed a MATLAB program for the determination of the optimal position and radius of a sphere in Hansen space based on solubility data,[36] which they have kindly made available to us. Fitting the soluble points in 3D space and considering all other states to be insoluble, we obtain the domain in which Fmoc-FF is soluble, represented by the blue sphere in Fig. 7. The coordinates of the center of this sphere correspond to the HSPs (δ_h, δ_p, $2\delta_d$) = (4.25, 7.10, 14.44). Any point outside the blue sphere can be considered an insoluble state for Fmoc-FF. As these conditions were established at a fixed concentration of Fmoc-FF, the soluble sphere will shrink with increasing concentration, and *vice versa*.

Next, we consider the different insoluble states. In Fig. 7, two separate gel domains (red) can be observed – one encompassing binary systems of Fmoc-FF in apolar solvents, and the other corresponding to ternary systems at moderate to high water concentrations in the mixture, centered at (0.3, 3.0, 27.6) and (7.1, 16.8, 17.75), respectively. The sphere denoting crystal formation (green) is positioned between the two gel spheres and has the coordinates (3.8, 11.9, 21.0). These domains facili-
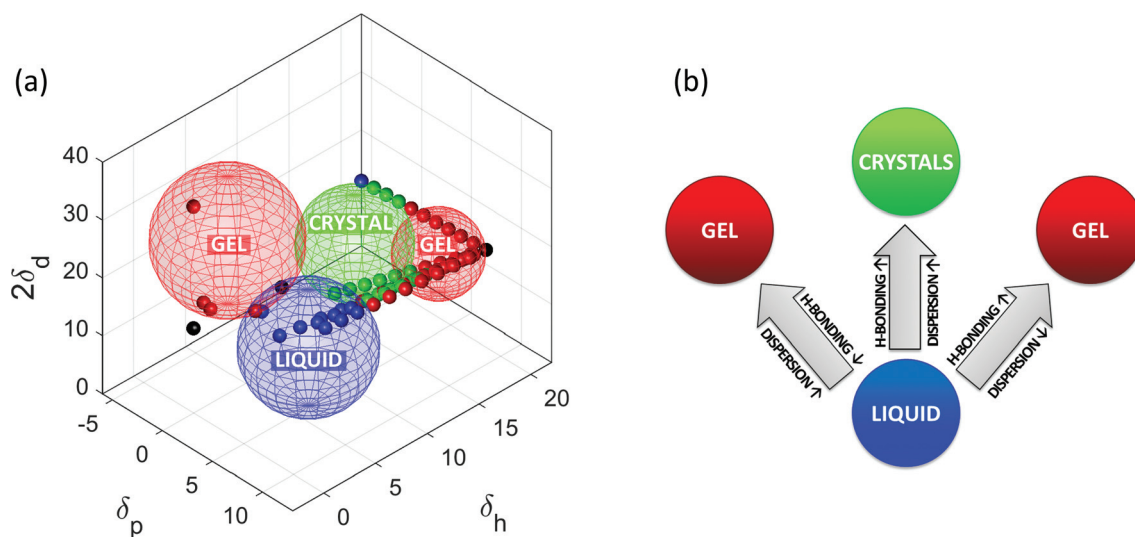

Fig. 7 (a) Domains of characteristic phase behavior presented in Hansen space (blue: liquid, red: gel, green: crystals) and (b) pathways to phase transition.

tate visualization and allow us to interpret solvent–solute interactions in light of the physical concepts behind the Hansen solubility parameters. Let us consider the structure of the amphiphilic Fmoc-FF molecule (Fig. 6f). The peptide backbone is prone to hydrogen bonding[14,22] due to the presence of hydroxyl and amino groups. On the other hand, the molecule will also display a highly hydrophobic, apolar character arising from the aromatic features, the interactions of which are primarily governed by dispersion forces. The ability of a particular solvent to solubilize an Fmoc-FF molecule can be thought of as the capacity of the solvent molecules to compete with other Fmoc-FF molecules at the featured interaction sites.

With this in mind, the gelation of Fmoc-FF in apolar solvents, such as benzene and toluene, can be understood as represented in Fig. 7. Shifting in Hansen space from the blue solubility sphere to the red gel sphere at (0.3, 3.0, 29.6), hydrogen bonding and polar capabilities of the solvents are reduced, and dispersion interactions are increased, allowing the peptide to be dissolved at elevated temperatures. Since there is no competition for hydrogen bonding between Fmoc-FF molecules, formation of β-sheets takes place as the temperature is lowered and intermolecular attractions are increased, and unidirectional growth proceeds *via* a combination of hydrogen bonding and π–π stacking.[14]

When shifting in Hansen space from the blue sphere to the other red gel sphere (7.1, 18, 17.75) in the direction of increasing δ_h, two possible effects can take place. First, decreasing dispersion forces moving from DMSO to water results in reducing competing interactions of the solvent with the aromatic groups of Fmoc-FF, allowing π–π stacking of the molecules to take over. Second, since there are now three components in the system (Fmoc-FF, solvent, and water), moving in the direction of increasing hydrogen bonding interactions can result in the competition of all three species. As the water concentration is increased, DMSO may preferentially hydrogen-bond with water, hence allowing the Fmoc-FF molecules to form hydrogen bonds between one another.

In both gelation pathways, the imbalance of the forces induces face-to-face interactions resulting in one-dimensional growth of fibers. Similar observations have been made in simulations of nucleation and growth of amyloid fibers, in which face-to-face interactions are favored and side interactions are limited by a non-parallel repulsive energy term to allow for unidirectional growth.[46–48]

A third case arises with the formation of large crystal aggregates (green sphere in Fig. 7). The increasing distance R from the blue sphere in the direction of the green sphere results in decreasing solubility. However, once the solubility boundary is crossed, the H-bond/polar and dispersion interactions are still balanced and therefore no preferential directional interaction will induce one-dimensional growth. Instead, formation of crystal aggregates with no preferred axis of growth will be favored. This is consistent with the expectation drawn from the role of differential surface energies of the ends and sides of the crystal giving rise to a quasi-one-dimensional nucleus for the gelling systems.[21]

Conclusions

We have demonstrated that the phase behavior of Fmoc-FF, a dipeptide derivative gelator molecule, in a solvent or mixture of solvents depends on a balance of interaction forces of all the molecules present in the system. While fibrous networks can be formed in a variety of solvents, the molecular order in these fibers differs across these systems. Furthermore, a discrete number of different fiber populations can exist within one system. In some solvents, the formation of anisotropic fibers is observed as a transient metastable state, followed by disassembly of fibers and formation of crystals with no preferred axis of growth. The ability of the system to transition from one state to the other depends on depth of the potential well and the height of barrier between the two free energy minima (Fig. 5). In DMSO/H_2O mixtures, large crystals are not attainable, indicating that the anisotropic interactions trap the molecules in a deep energy minimum.

While the fibrous network in DMSO/H_2O is virtually infinitely stable, the evidence of more than one structural conformation of Fmoc-FF indicates that the system is not in true equilibrium, as one or more kinetically trapped states exist.

In solvents such as methanol and ethanol, transitioning from fibers to large crystal aggregates is less costly at low water concentrations, rendering the fibrous gel state metastable. The imbalance of competing interactions of solvent molecules with the attractive sites of the gelator induces directional bonding of the solute molecules, resulting in anisotropic growth. Hence, in the design of a new self-assembling molecule with hydrogen bonding and π–π stacking capabilities, solvent–solute interactions will play a critical role in determining the structure, stability, and shelf life of the material.

Conflicts of interest

There are no conflicts to declare.

Acknowledgements

References

1 H. Löwen, *Phys. Rep.*, 1994, **237**, 249–324.

2 S. Berghmans, J. Mewis, H. Berghmans and H. Meijer, *Polymer*, 1995, **36**, 3085–3091.

3 R. M. L. Evans, W. C. K. Poon and M. E. Cates, *EPL*, 1997, **38**, 595.

4 A. Paravastu, A. Petkova and R. Tycko, *Biophys. J.*, 2006, **90**, 4618–4629.

5 A. Petkova, R. Leapman, Z. Guo, W. Yau, M. Mattson and R. Tycko, *Science*, 2005, **307**, 262–265.

6 Y. Miller, B. Ma and R. Nussinov, *Chem. Rev.*, 2010, **110**, 4820–4838.

7 T. Miti, M. Mulaj, J. Schmit and M. Muschol, *Biomacromolecules*, 2015, **16**, 326–335.

8 B. Guo, S. Kao, H. McDonald, A. Asanov, L. L. Combs and W. William Wilson, *J. Cryst. Growth*, 1999, **196**, 424–433.

9 B. L. Neal, D. Asthagiri and A. M. Lenhoff, *Biophys. J.*, 1998, **75**, 2469–2477.

10 A. M. Kulkarni and C. F. Zukoski, *Langmuir*, 2002, **18**, 3090–3099.

11 A. Y. Mirarefi and C. F. Zukoski, *J. Cryst. Growth*, 2004, **265**, 274–283.

12 G. He, R. B. H. Tan, P. J. A. Kenis and C. F. Zukoski, *J. Phys. Chem. B*, 2007, **111**, 12494–12499.

13 V. Jayawarna, M. Ali, T. Jowitt, A. Miller, A. Saiani, J. Gough and R. Ulijn, *Adv. Mater.*, 2006, **18**, 611–614.

14 A. Smith, R. Williams, C. Tang, P. Coppo, R. Collins, M. Turner, A. Saiani and R. Ulijn, *Adv. Mater.*, 2008, **20**, 37–41.

15 V. Jayawarna, S. Richardson, A. Hirst, N. Hodson, A. Saiani, J. Gough and R. Ulijn, *Acta Biomater.*, 2009, **5**, 934–943.

16 A. Mahler, M. Reches, M. Rechter, S. Cohen and E. Gazit, *Adv. Mater.*, 2006, **18**, 1365–1370.

17 R. Orbach, L. Adler-Abramovich, S. Zigerson, I. Mironi-Harpaz, D. Seliktar and E. Gazit, *Biomacromolecules*, 2009, **10**, 2646–2651.

18 N. Dudukovic and C. Zukoski, *Langmuir*, 2014, **30**, 4493–4500.

19 N. Dudukovic and C. Zukoski, *Soft Matter*, 2014, **10**, 7849–7856.

20 N. Dudukovic and C. Zukoski, *J. Chem. Phys.*, 2014, **141**, 164905.

21 N. Dudukovic and C. Zukoski, *Soft Matter*, 2015, **11**, 7663–7673.

22 R. Ulijn and A. Smith, *Chem. Soc. Rev.*, 2008, **37**, 664–675.

23 R. Mart, R. Osborne, M. Stevens and R. Ulijn, *Soft Matter*, 2006, **2**, 822–835.

24 S. Zhang, *Nat. Biotechnol.*, 2003, **21**, 1171–1178.

25 S. Kim, J. Kim, J. Lee and C. Park, *Small*, 2015, **11**, 3623–3640.

26 C. Chen, K. Liu, J. Li and X. Yan, *Adv. Colloid Interface Sci.*, 2015, **225**, 177–193.

27 T. Waku and N. Tanaka, *Polym. Int.*, 2017, **66**, 277–288.

28 J. Raeburn, C. Mendoza-Cuenca, B. Cattoz, M. Little, A. Terry, A. Cardoso, P. Griffiths and D. Adams, *Soft Matter*, 2015, **11**, 927–935.

29 J. Wang, K. Liu, L. Yan, A. Wang, S. Bai and X. Yan, *ACS Nano*, 2016, **10**, 2138–2143.

30 I. Sasselli, P. Halling, R. Ulijn and T. Tuttle, *ACS Nano*, 2016, **10**, 2661–2668.

31 D. J. Adams, K. Morris, L. Chen, L. C. Serpell, J. Bacsa and G. M. Day, *Soft Matter*, 2010, **6**, 4144–4156.

32 K. A. Houton, K. L. Morris, L. Chen, M. Schmidtmann, J. T. A. Jones, L. C. Serpell, G. O. Lloyd and D. J. Adams, *Langmuir*, 2012, **28**, 9797–9806.

33 C. Hansen and K. Skaarup, *J. Oil Colour Chem. Assoc.*, 1968, **51**, 76–79.

34 E. Stefanis and C. Panayiotou, *Int. J. Thermophys.*, 2008, **29**, 568–585.

35 K. Diehn, H. Oh, R. Hashemipour and S. Raghavan, *Soft Matter*, 2014, **10**, 2632–2640.

36 K. K. Diehn, H. Oh, R. Hashemipour, R. G. Weiss and S. R. Raghavan, *Soft Matter*, 2014, **10**, 2632–2640.

37 P. Curcio, F. Allix, G. Pickaert and B. Jamart-Gregoire, *Chem. – Eur. J.*, 2011, **17**, 13603–13612.

38 J. Bonnet, G. Suissa, M. Raynal and L. Bouteiller, *Soft Matter*, 2014, **10**, 3154–3160.

39 J. Gao, S. Wu and M. Rogers, *J. Mater. Chem.*, 2012, **22**, 12651–12658.

40 M. Raynal and L. Bouteiller, *Chem. Commun.*, 2011, **47**, 8271–8273.

41 Y. Lan, M. Corradini, R. Weiss, S. Raghavan and M. Rogers, *Chem. Soc. Rev.*, 2015, **44**, 6035–6058.

42 A. Pines, M. Gibby and J. Waugh, *J. Chem. Phys.*, 1973, **59**, 569–590.

43 A. Bennett, C. Rienstra, M. Auger, K. Lakshmi and R. Griffin, *J. Chem. Phys.*, 1995, **103**, 6951–6958.

44 T. Threlfall, *Org. Process Res. Dev.*, 2003, **7**, 1017–1027.

45 B. Roy, P. Bairi and A. Nandi, *Soft Matter*, 2012, **8**, 2366–2369.

46 J. Zhang and M. Muthukumar, *J. Chem. Phys.*, 2009, **130**, 035102.

47 S. Auer, *J. Phys. Chem. B*, 2014, **118**, 5289–5299.

48 I. Nyrkova, A. Semenov, A. Aggeli, M. Bell, N. Boden and T. McLeish, *Eur. Phys. J. B*, 2000, **17**, 499–513.

49 J. R. Moffat and D. K. Smith, *Chem. Commun.*, 2008, 2248–2250.